Binary droplet collision at high Weber number

Kuo-Long Pan,[*] Ping-Chung Chou, and Yu-Jen Tseng

Department of Mechanical Engineering, National Taiwan University, No. 1, Sec. 4, Roosevelt Rd., Taipei 106, Taiwan, Republic of China

By using the techniques developed for generating high-speed droplets, we have systematically investigated binary droplet collision when the Weber number (We) was increased from the range usually tested in previous studies on the order of 10 to a much larger value of about 5100 for water (a droplet at 23 m/s with a diameter of 0.7 mm). Various liquids were also used to explore the effects of viscosity and surface tension. Specifically, beyond the well-known regimes at moderate We's, which exhibited coalescence, separation, and separation followed by satellite droplets, we found different behaviors showing a fingering lamella, separation after fingering, breakup of outer fingers, and prompt splattering into multiple secondary droplets as We was increased. The critical Weber numbers that mark the boundaries between these impact regimes are identified. The specific impact behaviors, such as fingering and prompt splattering or splashing, share essential similarity with those also observed in droplet-surface impacts, whereas substantial variations in the transition boundaries may result from the disparity of the boundary conditions at impacts. To compare the outcomes of both types of collisions, a simple model based on energy conservation was carried out to predict the maximum diameter of an expanding liquid disk for a binary droplet collision. The results oppose the dominance of viscous drag, as proposed by previous studies, as the main deceleration force to effect a Rayleigh-Taylor instability and ensuing periphery fingers, which may further lead to the formations of satellite droplets.

PACS number(s): 47.55.df, 47.20.Dr, 47.20.Ma

I. INTRODUCTION

The collision dynamics between two droplets plays a crucial role in various disciplines of nature and practical interests, for example, in meteorological phenomena such as formation of rain drops, operation of nuclear reactors, spray combustion in liquid-fueled combustors, fire fighting via liquid injection, and relevant applications of spraying processes such as painting and coating. The scenarios have been widely investigated [1–4], showing characteristic transitions from coalescence to bouncing, to coalescence again, and to temporary coalescence followed by separation of primary droplets and further creations of satellite droplets when a governing dimensionless parameter of Weber number is increased, as defined by $We = \rho V_r^2 D / \sigma$, where V_r is the relative velocity; D is the diameter of the droplet; and ρ and σ are, respectively, the density and the surface tension of the liquid.

Although various regimes have been identified in the literature, those at relatively high We, say, larger than 100, have rarely been explored. Such a strong impact would yield substantial disintegration into secondary droplets and certainly are crucial for applications relevant to splattering of initial masses such as spraying processes in liquid-fueled combustors, specifically near the critical condition where the surface tension becomes relatively low, and to thermal spray processes where molten droplets are propelled onto a surface by a high-temperature jet. Based on the general understanding of the impaction mechanism via broadly investigated phenomena of "splashing" that has been extensively studied in the collisions of droplets upon either dry or wet surfaces [5–9], it is expected that similar phenomena could also appear in binary droplet collision. Indeed, such a possibility has

been revealed from a pioneering work on this subject four decades ago [10]. However, the unique regime was merely captured in a qualitative manner via limited controllability for desired well-conditioned (stable and spherical) droplets and visual recording technique available during that era (through which milk was added in water to facilitate observation). None has so far succeeded in the study to provide a clearer elucidation and a systematic investigation.

In this paper, we report an experimental study regarding the collision characteristics with strong impact between two droplets that are distinct from but share somewhat similarities with those of droplet-surface collisions. Specifically, in such a condition that can be characterized by a high Weber number, the impinging interfaces may lead to expansion of a flattened lamella of liquid and to scattering of multiple satellite droplets from the periphery, known as splashing in the extensive studies of droplet-surface impact [11]. Similar behaviors were observed in our study of binary droplet collision, whereas the underlying mechanism was not subjected to the sophisticated effects of backing surfaces as encountered in the droplet-surface configuration. We have systematically investigated the regimes as We is increased from the generally tested range on the order of 10 to that much higher, about 5100. To achieve the test condition of such a harsh impact, we have developed two methods for generating high-speed droplets. They are different from conventional approaches adopting such techniques as vibration of piezoelectric diaphragms [1,2] or creation of multiple droplets due to the Rayleigh instability either via wave modulation [12,13] or naturally during free dripping [6,7], by which the droplet speed is usually on the order of 1 m/s. By means of the present cutting technique for a high-speed jet and the droplet carrying method based on a strong air flow, we can create moderately stable droplets with a velocity of up to 23 m/s and, hence, with a Weber number of about 5100 for water.

*panpeter@ntu.edu.tw

II. EXPERIMENTAL SPECIFICATIONS

A. Cutting of a high-speed jet

The setup of our first experimental approach is similar to that described in [9] by which a water jet with an adjustable speed was generated by the thrust of a gas cylinder driven by a compressor, which was equipped with a movable piston linked to two liquid cylinders. Due to compression, the liquid within the two smaller cylinders downstream was injected out. The jet, passing through filters and eventually squeezed out of a nozzle with a given exit diameter of 0.45 mm, was continuously discharged into a chamber that was made of Plexiglas walls and used to isolate the influence of external air. The high-speed jet was then cut by a knife edge on a rotating disk to form a separate mass. With a fine adjustment of the rotation speed of the disk and upstream pressure, a stable droplet with trivial oscillation moving at a desired high speed can be established before hitting the target droplet. We note that the speed of the fastest droplet that became nearly spherical and stable was 23 m/s, which was not in an oscillating manner as in other studies that might yield uncertain effect of internal flow. The attainment of the maximum speed was limited by the necessary distance for the relaxation of initially induced oscillation of the droplet and the deceleration due to viscous drag of surrounding air, which reduced the droplet speed with increasing traveling distance. Furthermore, to generate a binary droplet collision at the desired head-on direction with a least uncertainty, the other droplet was created by a well-controlled technique via the vibration of a piezoelectric diaphragm. The collision was usually performed when this droplet shot upward was at the vertex of its trajectory and had a negligible velocity.

B. Droplet carried by a high-speed flow

To avoid unnecessary consumption when using liquids other than water and to further increase the chance of head-on collisions between two droplets approaching each other at a relatively high velocity, the second method was developed. As illustrated by the schematic in Fig. 1, a flow created upstream by a compressor passes through a porous metal plate after which higher uniformity is obtained; it is then joined by a stable droplet injected from a piezoelectric-diaphragm generator. The flow was accelerated via a contraction nozzle whereby the droplet could be centered in the downstream pipe with a diameter of 2 cm. After sufficient relaxation in the long enough chamber, a stable droplet moving at nearly the speed of the high-speed air flow can be formed. In order to collide with another droplet without the influence of the surrounding flow, the droplet was introduced into a closed tank through a small hole with a diameter of 1 mm such that the high-speed flow was diverted away prior to the tank. Due to a substantial change in the static pressure, however, the collision had to be made early enough to avoid significant deformation of the incoming droplet. Since the generation of the two droplets can be controlled by the delay circuit of the electronic control system, satisfactory sphericity and stability of the droplets were ensured before the impact. The results obtained by the two different techniques have shown a very close agreement, whereas the second
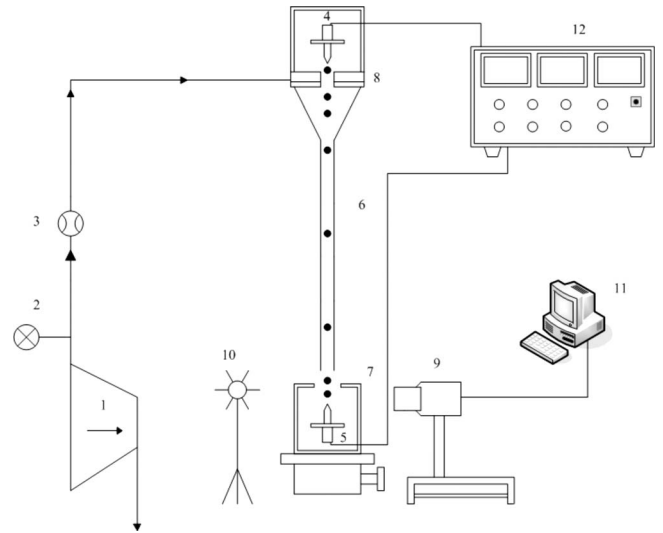

FIG. 1. Schematic of the experimental setup for droplets carried by a high-speed flow. 1: air compressor; 2: pressure controlling valve; 3: flow meter; 4 and 5: droplet generators; 6: contraction and acceleration sections; 7: enclosed test section; 8: upstream tank with porous medium filter; 9: high-speed camera; 10: LED lamp; 11: personal computer; 12: electronic control box.

method was adopted for various fluids with distinct properties such as surface tension and viscosity (as listed in Table I). Furthermore, the successful rate of attaining a head-on collision was significantly higher, almost up to 70%. To present clearer images, however, the following pictures were captured by the first method because the test section of the second approach was somewhat obscured by the enclosure wall made of Plexiglas.

The sequential pictures were recorded by a high-speed complementary metal-oxide semiconductor (CMOS) digital camera (X-Stream™ Vision, XS-4) up to a frame rate of 20 000 frames/s in a resolution of 128×512. The images presented herein were mostly captured with a spatial resolution of one pixel corresponding to 0.0526 mm, which was much smaller than the sizes of tested droplets. The camera was synchronized with a light-emitting diode (LED) lamp that can support the shortest exposure time of 1 μs, so as to capture transient images in such a rapid motion with sufficiently small exposure and enough light intensity while avoiding blurring due to the background scattering.

TABLE I. Fluid properties of tested liquids.

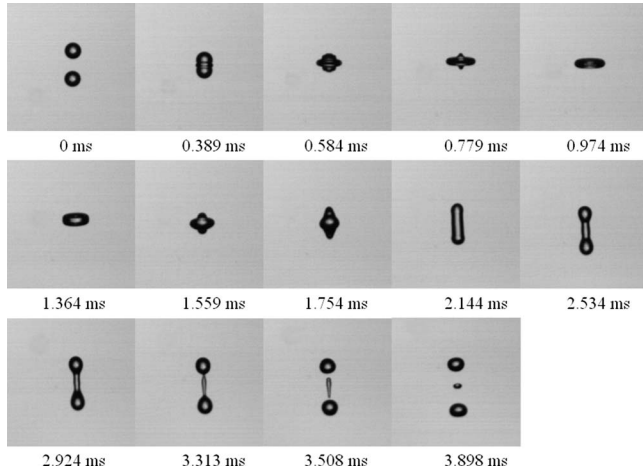|	Viscosity μ (10^{-3} N s/m^2)	Surface tension σ (10^{-3} N/m)	Density ρ (kg/m^3)
Water	1.000	72.0	1000.0
Heptane	0.409	20.1	684.0
Nonane	0.665	22.8	722.0
Propanol	1.950	25.2	799.6
Hexanol	4.580	27.8	815.3
Glycerine 40%	5.160	68.9	1103.2
Glycerine 57%	10.600	67.3	1149.9

FIG. 2. The collision sequence between two water droplets showing temporary coalescence followed by separation and satellite droplets (We=58, V_r=2.45 m/s, D=0.7 mm).

III. RESULTS AND DISCUSSION

A. Collision dynamics at high Weber number

We have performed a series of collision tests for two identical water droplets from low to high Weber numbers. Starting with a lower We on the order of 10, we sequentially justified the regimes of nominally classified permanent coalescence, separation, and separation with satellite droplets that have been considerably investigated and understood [1–3] and therefore not repeated herein. To facilitate the following discussion, however, the evolution of temporary coalescence followed by separation and satellite droplets is presented in Fig. 2 for later comparison. It shows the disintegration of the merged droplets after the lamella retracts and elongates, in order to redistribute the excess energy that cannot be contained in a single mass mainly in the form of surface energy and viscous dissipation to the energies of separated droplets and satellites (t=3.898 ms) that are further created when We is increased.

In our experiment, significantly higher We's were obtained and various transitions not observed before could be captured via the current high-speed photography. Specifically, as We is increased [Fig. 3(a)], the periphery of the expanding disk after impact is wrinkled (t=0.975 ms), which has been argued to initiate from the Rayleigh-Taylor instability [14,15] or a rim transverse instability [16] observed in the collision between a droplet and a rigid surface, and fingering structure is subsequently formed (t=1.754 ms). Furthermore, a thin film is ostensibly visible (e.g., t=1.754 and 2.144 ms) on the center plane surrounded by the thicker rim, while a torus structure should have been formed in the regimes at lower We's [1]. After that, satellite droplets are not generated as the regime of separation with satellite droplets at lower We as that shown in Fig. 2 in which fingers are not formed, indicating an increased viscous dissipation that digests more of the energy content. When We is further increased, by the increase in the initial impact energy, the merged droplet has to disintegrate, also concomitant with satellite droplets at sufficiently large We, so as to bal-
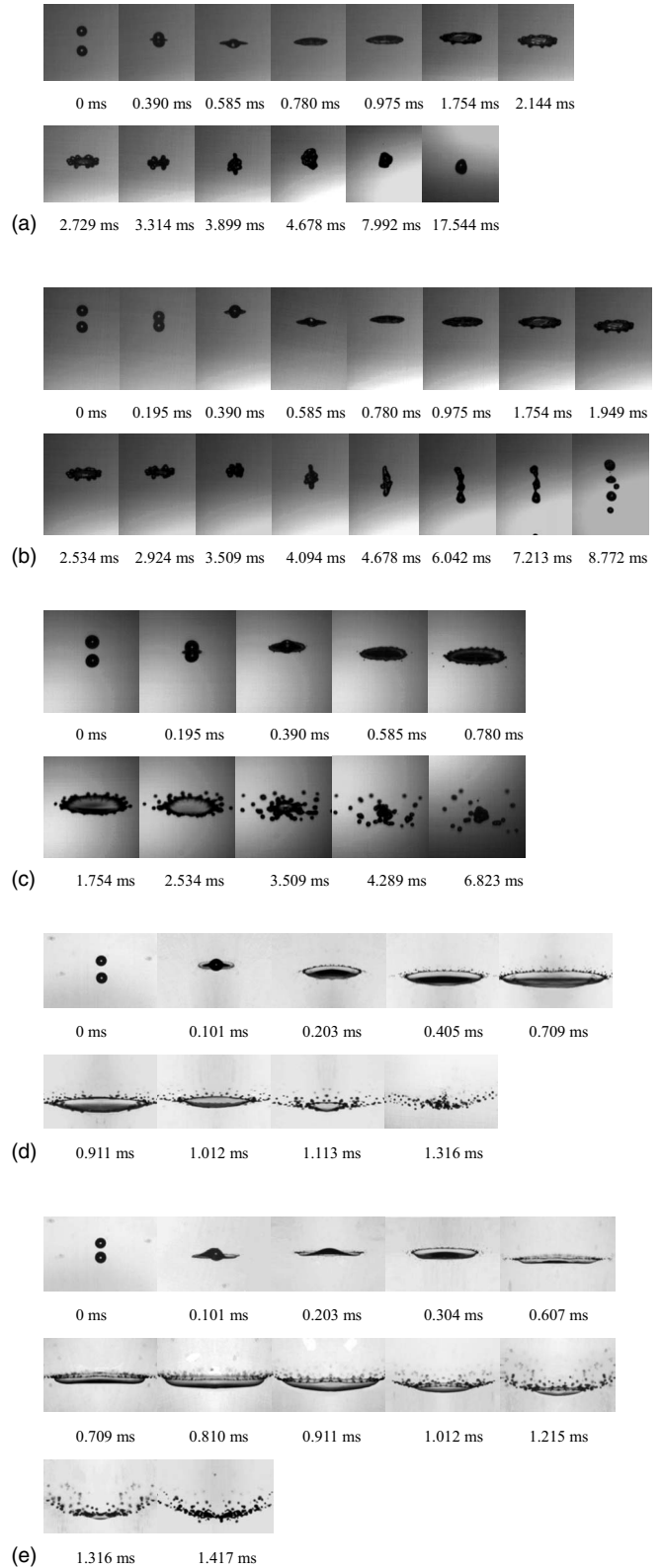

FIG. 3. The collision sequence between two water droplets showing (a) fingering (We=210, V=3.89 m/s, D=1.0 mm); (b) fingering and separation (We=277, V_r=4.26 m/s, D=1.10 mm); (c) breakup (We=878, V_r=9.50 m/s, D=0.70 mm); (d) prompt splattering (We=1593, V_r=12.80 m/s, D=0.70 mm); (e) prompt splattering (We=5144, V_r=23.00 m/s, D=0.70 mm).

ance additional energy that cannot be maintained in the single mass formed after the expanding disk contracts. It is thus designated as "fingering and separation" as shown in Fig. 3(b). If We is further raised, the fingers at the rim of the lamella break, leading to scattering of multiple secondary droplets [Fig. 3(c), $t=0.585$ ms], as designated by a "breakup" or a "splattering" regime. Secondary droplets will be continuously generated when the disk expands and then retracts. Eventually, when the disk is small enough, multiple droplets would be formed due to disruption of the thin film in addition to the splattering of secondary droplets from the circumference, as can be seen from the later evolution. In contrast to that in the collision of a droplet upon a solid surface [15], which shows multiple holes on the center film due to nonuniformity related to surface roughness, the film on the center plane formed by the collision of two droplets looks smooth for quite a long time [also demonstrated in Figs. 3(d) and 3(e)]. It then collapses when the radius becomes so small that the converging of the wrinkled rim with fingers leads to a substantial disintegration into many pieces and hence to secondary droplets.

In passing we note that because of unequal velocities generated by the different droplet generators, the outer part of the expanded disk is "bent" upward by the surrounding air, particularly when the primary droplet moves at such a high velocity downward as shown in Figs. 3(d) and 3(e).

B. Splattering characteristics

The radius at which the fingers are broken into secondary droplets increases first with higher We and then decreases because the initiation instant of its occurrence during the collision process is advanced with an increased We. That is, the breakup of the fingers is first created when the disk is contracting, whereas the outer liquid segments may still have somewhat outward inertia such that they are pinched off by the pulling of the retracting disk, as shown in Fig. 4(a). If We becomes larger, however, the outward momentum of emitted fingers is magnified; as a consequence, the initiation for breaking becomes earlier and hence the radius of occurrence is larger. Enlarged with an increased We of up to about 800, the breakup happens when the expanding disk develops to its maximum radius before retraction [Fig. 4(b)]. After that, the critical radius is attained as the lamella is expanding and becomes smaller with higher We. The diameter whence breakup is initiated (D_b), normalized by the droplet size and designated as β, is plotted in Fig. 5 with respect to We. In addition, the boundaries between distinct regimes for head-on binary droplet collision are also marked off in the figure.

An intriguing phenomenon was observed at a critical We whence breaking of circumferential fingers occurred immediately when a sheet was ejected from the waist of merged droplets right after the impact [see Fig. 3(d)]. This astonishing event can be clearly identified if the view is zoomed in, as shown in Fig. 6, whereby lens of larger magnification was mounted onto the high-speed camera. Figure 6(a) shows that a thin disk with a continuous smooth rim expands outward, similar to a far view of Saturn, while secondary droplets are
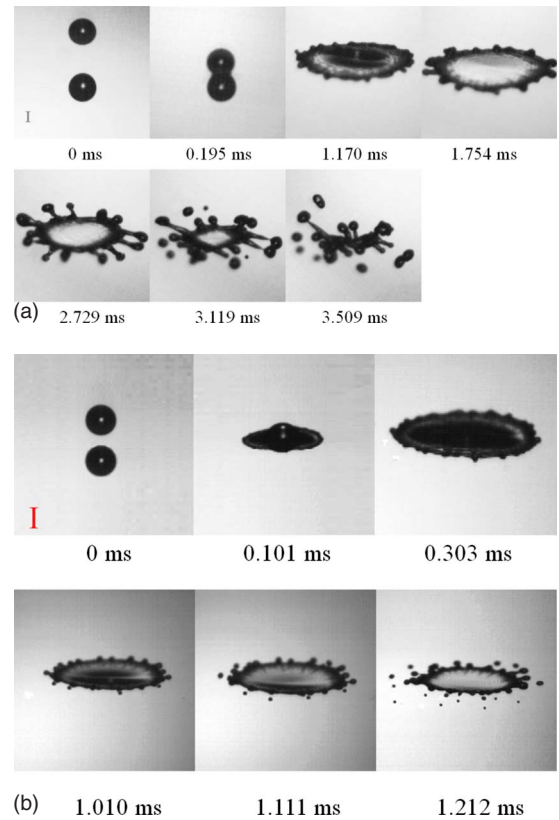

FIG. 4. (Color online) The collision sequences of two water droplets for (a) splattering at the receding phase (We=442.3, V_r=5.13 m/s, D=1.21 mm) and (b) splattering at the expanding phase with radius about the maximum (We=805.2, V_r=9.10 m/s, D=0.70 mm). Scale bar=0.50 mm.

scattered out if the radius becomes large enough (e.g., t=0.152 ms). With a higher We, however, the fracture is created almost immediately after the contact whereby a sheet is just squeezed out [Fig. 6(b), t=0.051 ms]. The exact instant of such splattering could not be distinguished within the smallest time resolution, i.e., 0.051 ms; but an image re-
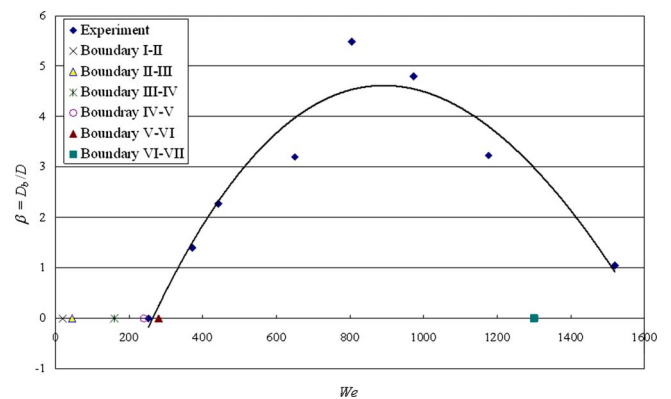

FIG. 5. (Color online) The variation in breakup diameter (D_b) normalized by droplet diameter β versus Weber number, fitted with a third-order polynomial. The boundaries separating different regimes are also marked at the axis, indicating Regime I: coalescence, II: separation, III: separation with satellite droplets, IV: fingering, V: fingering and separation, VI: breakup, and VII: prompt splattering.
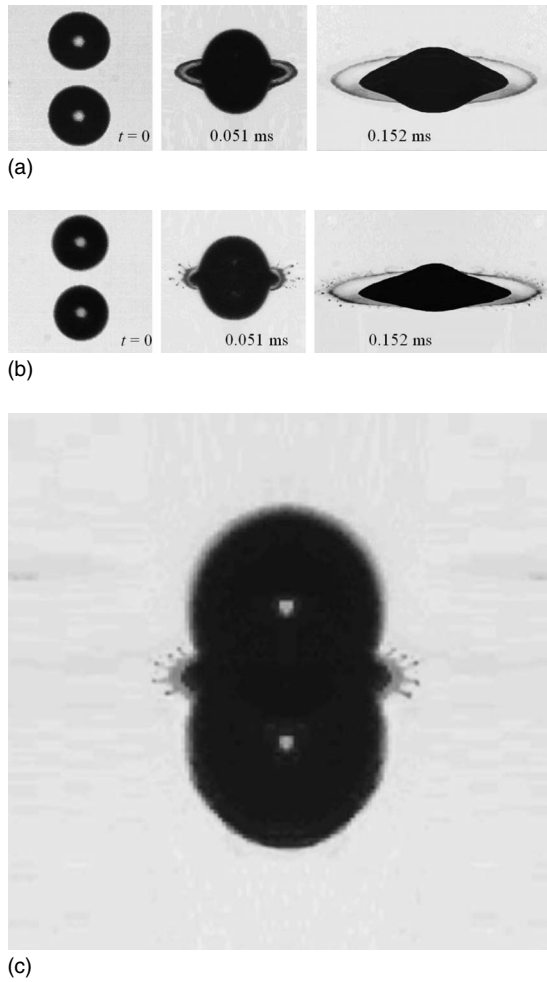
(a)

(b)

(c)

FIG. 6. The collision sequences of two water droplets for (a) splattering at the expanding stage (We=1176, V_r=11.00 m/s, D=0.70 mm) and (b) prompt splattering (We=1520, V_r=12.50 m/s, D=0.70 mm). (c) shows the transient image that was once captured almost immediately after the impact at the same condition as (b).

corded in a different sequence was ever captured, showing its occurrence at a very early stage [Fig. 6(c)]. New droplets are continuously created during the process when the disk expands and then retracts due to the breakup of outer fingers. We thus define the regime as "prompt splattering." By comparing Figs. 4 and 6, it is also seen that the sizes of satellite droplets are generally reduced with raised Weber number. This would be related to thinner fingers that are created at the periphery whose diameters can be correlated with the thickness of the lamella or the size of the cross section of the rim bounding a free liquid sheet, as analyzed by Roisman *et al.* [16] for the upraising free sheets generated by single drop impacts onto a rigid surface. Further investigation is needed to clarify the structure in a binary droplet collision. When We is further increased, the scenario is essentially the same and no particular transition can be identified, as shown in Fig. 3(e).

The plot of β versus We is shown in Fig. 7(a) for various fluids, which shows a similar trend with that of water (also plotted in Fig. 5) but shifted with varied scaling factors such
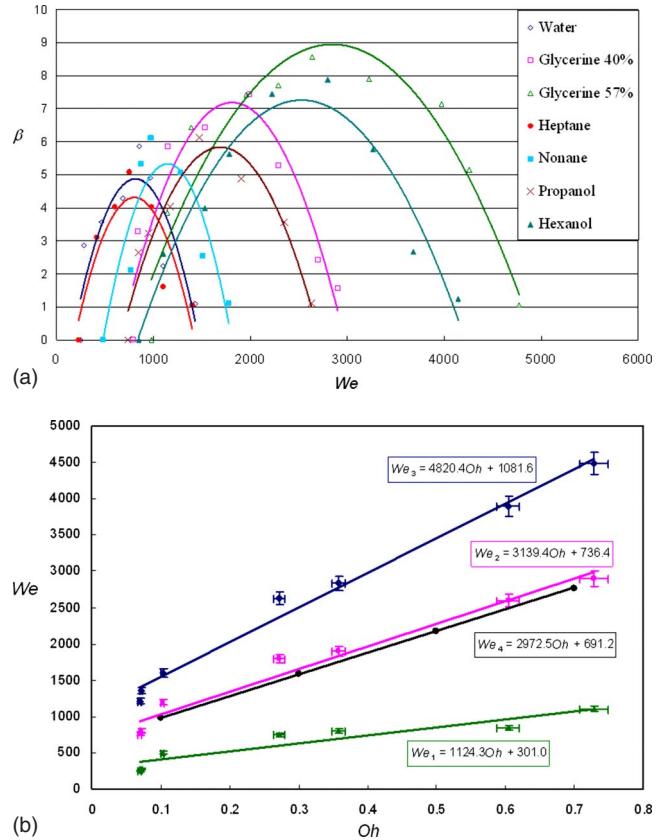

(a)

(b)

FIG. 7. (Color online) (a) The variation in normalized breakup diameter ($\beta = D_b/D$) with respect to We for different fluids, also fitted by polynomial lines; (b) critical We's versus Oh, also fitted by straight lines.

as span width and height. Since liquid viscosity is another parameter of importance, which may affect the extent of energy dissipation due to the liquid motion [2–4,17] and hence the transitional Weber numbers, we plot in Fig. 7(b) the initiation Weber numbers of breakup (We$_1$), splattering at the maximum radius (We$_2$), and prompt splattering (We$_3$) with respect to the Ohnesorge number Oh$=16\sqrt{2}\mu/(\rho\sigma D)^{1/2}$, which is proportional to (We)$^{1/2}$/Re, where Re$=\rho V_r D/\mu$ is the Reynolds number and μ is the viscosity of the liquid. It is seen that the variations can be simply fitted by straight lines. Furthermore, the curves in Fig. 7(a) are basically like symmetric parabolas because the arithmetic mean (We$_4$) of the two ends—i.e., the beginnings of the breakup and the prompt splattering represented, respectively, by We$_1$ and We$_3$—is quite in line with the fitting curve for We$_2$ as shown in Fig. 7(b).

C. Comparison with droplet-surface collision

It is of interest to compare the results of binary droplet collision with the impact of a droplet upon a dry solid surface. In this situation, when We is increased, the outcome changes from spreading of a lamella, to fingering at the periphery, and to emission of secondary droplets from the rim. The basic mechanisms have been well known to the community [8,11]. However, the quantitative boundaries of these
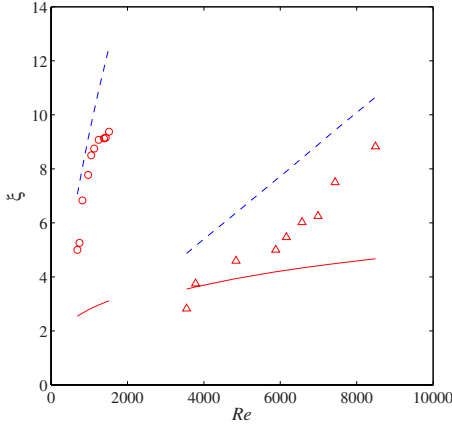
FIG. 8. (Color online) The variation in maximum spread factor ($\xi=D_e/D$) versus the Reynolds number. The triangles represent the measured data for collisions between two droplets made of water and the circles represent those made of water-57% glycerine. The solid lines are the predictions of Pasandideh-Fard *et al.* [19] for droplet-surface collision and the dashed lines are those of our present model in the corresponding ranges of measured We and Re for binary droplet collision.

transitions are complicated by the properties of the supporting solid surface such as the material and roughness. Consequently, the transition boundary of fingering to the breakup could be varied substantially when the roughness is different. Such complications would be reduced if the target plate is small [18] or even removed if the surface is not present in the colliding geometry. The symmetrical collision between two identical droplets as studied herein thus provides an ideal inviscid paradigm for investigating the fundamental structure of such an event.

By a comparison for the maximum diameter of an expanding disk (D_e), in terms of a spread factor defined as $\xi =D_e/D$, it is found that the binary droplet collision generically yields a clearly larger value than that of droplet impact upon a solid surface. This is shown in Fig. 8, which compares our measured data for the former made of water and its solution with 57% glycerine to the analytical prediction of Pasandideh-Fard *et al.* [19] for the latter, $\xi =\sqrt{(\text{We}+12)/[3(1-\cos\theta)+4\text{We}/\sqrt{\text{Re}}]}$, by using a typical contact angle for water on a metal surface $\theta=110°$ (not much different from that using a general assumption of $\text{We}\gg\sqrt{\text{Re}}$ and approximated by $\xi=0.5\,\text{Re}^{1/4}$), whose accuracy has been justified by the experiments of Mehdizadeh *et al.* [15] for droplet-surface collision. The disagreement is ostensibly due to the lack of significant viscous drag at the colliding plane between two droplets, which is nevertheless inherent on the solid surface associated with no-slip boundary condition and an essential boundary layer. A relevant demonstration can be referred to the numerical simulations presented in [4,20] for the velocity field after merging and disappearance of the impinging interfaces of impact droplets, showing a relatively lower dissipation in the center region than the others rendered large velocity gradients and hence viscous stresses.

To estimate the maximum spread factor fit for the binary droplet collision, we have conducted a simple analysis by including adequate viscous dissipation during the evolution
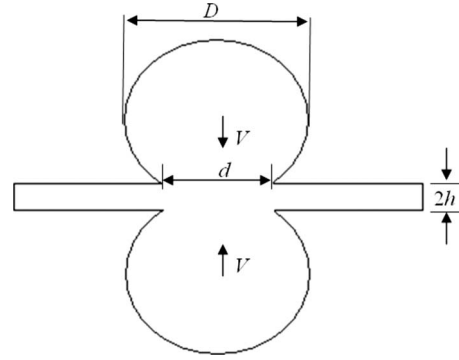

FIG. 9. Impact configuration of the model for expansion of coalesced droplets.

of an expanding disk. Based on the energy conservation, the sum of initial kinetic energy (E_K) and surface energy of the droplets (E_S) is equal to that of maximum deformation energy (E_{Sm}) and viscous dissipation during the spreading process (Φ_e), assuming negligible kinetic energy at the maximum extent of expansion, i.e.,

$$E_K + E_S = E_{Sm} + \Phi_e. \tag{1}$$

The first two terms are, respectively, equal to $\pi\rho D^3V^2/6$ and $2\pi\sigma D^2$ where the initial droplet velocity $V=1/2V_r$. The shape of the expanding disk is assumed to follow a cylindrical form with a uniform thickness $2h$ that can be estimated by the mass conservation as

$$h = \frac{D^3}{3D_e^2}, \tag{2}$$

which has been adopted to model the spreading process in the work of Pasandideh-Fard *et al.* [19] for droplet impact on a solid surface and found to yield satisfactory agreement with the experimental results. Due to the essential similarity of geometry on the half plane, the simplified configuration is also adopted herein for binary droplet collision, as illustrated in Fig. 9. As a consequence the surface energy at the maximum deformation can be approximated as

$$E_{Sm} = (2\pi D_e h + \pi D_e^2/2)\sigma. \tag{3}$$

The viscous dissipation energy is given by

$$\Phi = \mu \int_0^t dt \int \frac{1}{2}\left(\frac{\partial v_i}{\partial x_j} + \frac{\partial v_j}{\partial x_i}\right)^2 (dx)^3. \tag{4}$$

Following the estimation of Jiang *et al.* [2] that was also demonstrated in [3], the dissipation loss during the expansion process can be approximated by

$$\Phi_e \approx \mu\left(\frac{V}{h}\right)^2\left(\frac{\pi h d^2}{2}\right)t_e. \tag{5}$$

Here d is the diameter of the projected circle of the truncated sphere from which the liquid flows into the film of maximum velocity gradient, and the average value is taken to be $D/2$ because it varies between 0 and D in the period [19]. Also, the time to reach the maximum expansion, t_e, is calculated to
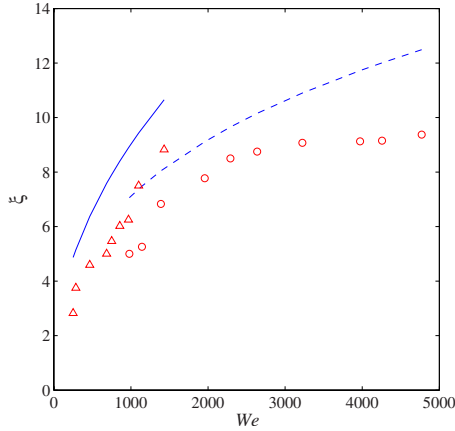
FIG. 10. (Color online) The variation in maximum spread factor ($\xi = D_e/D$) versus the Weber number. The triangles represent the measured data for collisions between two droplets made of water and the circles represent those made of water-57% glycerine. The solid and the dashed lines are the predictions of our present model, respectively, for these two liquids.

be $(8/3)D/V_r$. By substituting these quantities and Eq. (2) in Eq. (5), we obtain

$$\Phi_e \approx \pi \mu V D_e^2/2. \qquad (6)$$

Consequently, the energy conservation (1) can be written as

$$\left(\frac{1}{2} + \frac{\text{Re}}{\text{We}}\right)\xi^3 - \text{Re}\left(\frac{1}{12} + \frac{4}{\text{We}}\right)\xi + \frac{4}{3}\frac{\text{Re}}{\text{We}} = 0. \qquad (7)$$

The solution of Eq. (7) based on various combinations of We and Re measured in our experiments is plotted in Fig. 8. It is seen that our model has caught the essential features of ξ, specifically its variation with increasing Re that also accounts for various We's in the measured conditions since the dissipation loss evaluated for the binary droplet collision has been incorporated in the simple but straightforward analysis. In contrast to that of Pasandideh-Fard *et al.* [19] derived for the collision between a droplet and a solid surface that yields no-slip condition at the contact surface (corresponding to the center plane of the present geometry), the viscous dissipation is much smaller and hence the expansion diameter becomes larger. The dependence on the Weber number is also presented, as shown in Fig. 10, which indicates the increasing trend of ξ with larger We. Due to the simplicity of the model, however, there are inevitably some insufficiencies for the prediction and thus limited accuracy leading to the presented overestimation of ξ. It is likely related to the prediction of dissipated energy that might have been underestimated. To better describe the results, the viscous dissipation and the surface energy at the maximum deformation have to account for the detailed evolution of the geometry such as the torus with a center film and the fingering structure that may render more dissipation loss particularly at higher We and Re when its formation is further amplified. A more comprehensive analysis has been conducted in Ref. [21]; it was however found recently to yield inconsistent physical consequences due to negative kinetic energy that could be caused by overestimation of the viscous loss [22], which should be quite

sensitive to the assumed flow structure and critical for the resultant energy budget. Regarding the complicated mechanisms and sensitivity of viscous dissipation, the present model would provide a preliminary insight to the evolution of an expanding disk in spite of its much simplified configuration, whereas a complete theory for the binary droplet collision is still needed and being undertaken.

It was proposed in [14] that, for a droplet impacting a rigid surface, the viscous drag along the surface provided the deceleration of the interface moving toward the lighter medium of gas and thus caused the Rayleigh-Taylor instability that initiated the fingers at the periphery. Interestingly, in the absence of a contact surface, fingering structure was still observed in the present binary droplet collision and appeared even at a lower We ($\gtrsim 160$) than that of a water droplet impacting a smooth surface with the same Oh (We $\gtrsim 743$, as reported in [23]); consequently, the breakup regime whence secondary droplets were scattered out of the rim was also initiated at a lower We (≈ 280 and 2456, respectively, for the two configurations). As a result, it could be inferred that the liquid viscosity alone would not suffice to effect wrinkling of the rim since no substantial viscous retardation was ever present (or insignificant considering the trivial viscous drag of the surrounding air) near the center plane in the collision between two droplets, so as to trigger the instability like that assumed to occur in the droplet-surface collision [11]. Furthermore, if it were merely this mechanism to dominate the evolution, the deceleration would need an order of $-160g$ (g is the gravity acceleration) to match the experimental evidence [24], which obviously looks too large. This conclusion could support such theories as that proposed recently in [15,25], which have excluded the viscous effect that might have played merely a secondary role in the incipient development of Rayleigh-Taylor instability and accounted mainly for the balance between the capillary force and the inertia under the variation in evolving interfacial geometry such as interface length and curvature. Moreover, as stated in Ref. [26], to fit the wave numbers observed at the very beginning on the basis of a Rayleigh-Taylor instability when azimuthal undulations had been generated, it would need a tremendous deceleration to drive the instability and create wrinkling. This seemed not likely to be caused simply by the liquid viscosity in such a short duration and was supposed to be dominated by the capillary forces for the rapidly decelerating annular ring of fluid that first touched the surface.

After all, to illustrate the deceleration needed to drive a Rayleigh-Taylor instability effective for the formation of ensuing fingers, the active roles of surface tension and inertia played in the temporal development with nontrivial geometrical effects have to be accounted. Considering the rim structure at the periphery of the expanding disk, a refined mechanism was proposed recently based on the evolution of a rim transverse instability [16]. It involves the moment of forces associated with the inertia of the liquid entering the rim and could also interpret the onset of fingering and hence its role in splashing in the collision scenario of a droplet impinging a target surface or another droplet.

IV. CONCLUDING REMARKS

We have developed a method, supplementary to our prior technique based on the cutting of a high-speed jet, for gen-

erating a high-speed binary droplet collision, nominally up to 23 m/s. Different from conventional approaches in terms of vibration of piezoelectric diaphragms or creation of multiple droplets due to the Rayleigh instability either via wave modulation or naturally during free dripping, by which the produced droplet speed is typically on the order of 1 m/s, the methodology is based on transmittal of a high-speed flow for an initially stable droplet. In contrast to the cutting-jet method, although yielding a similar highest Weber number for a stable water droplet of about 5100, the present approach allows for an easy replacement of different fluids as well as a higher successful rate of head-on collision between two droplets and hence a wide variety of parametric conditions.

Both of these two techniques were adopted to investigate the collision between two droplets and specific patterns were found such as the fingering rim of a flattened disk and an ensuing breakup, which were somehow analogous to that extensively observed during the impingement of a droplet upon a solid surface. The formation of fingering structure further increased viscous dissipation inside the liquid and reduced the propensity of the merged droplets to separate again. When We became larger, however, separation of the coalesced droplet and following disintegration into satellite droplets as that generally identified at lower We were yielded so as to balance the excess energy. An intriguing structure of splattering was observed if We was further increased whereby the outer fingers were broken. The critical radius of breakup was found to increase first with an increased We and then decreased. When a specific We was approached, breaking of the droplets occurred immediately after the impact of the two droplets, whence multiple droplets were continuously shed out from the rim of the ejected sheet during its ensuing expansion and contraction. This structure of prompt splattering was observed to happen as We $\gtrsim$ 1300 for water, and no more specific transition was captured up to the limit of the experimental conditions.

The transition boundaries for fingering and splattering that happen at high We's and have not been quantitatively or even qualitatively (the former) investigated for binary droplet collision also provide symmetric paradigms for further unveiling the fundamental structure of a droplet impacting a rigid dry surface, without influences of surface roughness and material effects, which has a similar half plane but no-slip condition at the center surface. Although similar fingering structure is also created, even more easily (formed at a lower We), the viscous dissipation, however, is much smaller in the collision between two droplets due to full-slip condition at the center plane. It implies that the viscous drag could not be the essential mechanism to trigger the Rayleigh-Taylor instability and to cause wrinkling of the periphery and ensuing fingers, as claimed by previous studies. This would necessitate active roles of other mechanisms such as the capillary forces associated with geometrical variations.

[1] N. Ashgriz and J. Y. Poo, J. Fluid Mech. **221**, 183 (1990).

[2] Y. J. Jiang, A. Umemura, and C. K. Law, J. Fluid Mech. **234**, 171 (1992).

[3] J. Qian and C. K. Law, J. Fluid Mech. **331**, 59 (1997).

[4] K. L. Pan, C. K. Law, and B. Zhou, J. Appl. Phys. **103**, 064901 (2008).

[5] A. M. Worthington, *A Study of Splashes* (Longmans, Green, London, 1908).

[6] P. V. Hobbs and A. J. Kezweeny, Science **155**, 1112 (1967).

[7] F. Rodriguez and R. Mesler, J. Colloid Interface Sci. **106**, 347 (1985).

[8] A. L. Yarin, Annu. Rev. Fluid Mech. **38**, 159 (2006).

[9] K. L. Pan, K. R. Cheng, P. C. Chou, and C. H. Wang, Exp. Fluids **45**, 435 (2008).

[10] R. Gunn, Science **150**, 695 (1965).

[11] M. Rein, Fluid Dyn. Res. **12**, 61 (1993).

[12] O. W. Jayaratne and B. J. Mason, Proc. R. Soc. London, Ser. A **280**, 545 (1964).

[13] J. R. Adam, N. R. Lindblad, and C. D. Hendricks, J. Appl. Phys. **39**, 5173 (1968).

[14] R. F. Allen, J. Colloid Interface Sci. **51**, 350 (1975).

[15] N. Z. Mehdizadeh, S. Chandra, and J. Mostaghimi, J. Fluid Mech. **510**, 353 (2004).

[16] I. V. Roisman, K. Horvat, and C. Tropea, Phys. Fluids **18**, 102104 (2006).

[17] K. L. Pan and C. K. Law, J. Fluid Mech. **587**, 1 (2007).

[18] A. Rozhkov, B. Frunet-Foch, and M. Vignes-Adler, Phys. Fluids **14**, 3485 (2002).

[19] M. Pasandideh-Fard, Y. M. Qiao, S. Chandra, and J. Mostaghimi, Phys. Fluids **8**, 650 (1996).

[20] K. L. Pan, Ph.D. thesis, Princeton University, 2004.

[21] I. V. Roisman, Phys. Fluids **16**, 3438 (2004).

[22] K. L. Pan and I. V. Roisman, Phys. Fluids **21**, 022101 (2009).

[23] K. L. Pan, K. C. Tseng, and C. H. Wang, Exp. Fluids (to be published)

[24] A. L. Yarin and D. A. Weiss, J. Fluid Mech. **283**, 141 (1995).

[25] H. Y. Kim, Z. C. Feng, and J. H. Chun, Phys. Fluids **12**, 531 (2000).

[26] S. T. Thoroddsen and J. Sakakibara, Phys. Fluids **10**, 1359 (1998).